Electron Transfer, Linkage Isomerization, Bulk Magnetic Order, and Spin-Glass Behavior in the Iron Hexacyanomanganate Prussian Blue Analogue

Wayne E. Buschmann,[a] Jürgen Ensling,[b] Philipp Gütlich,[b] and Joel S. Miller*[a]

Abstract: The reaction of $[Fe^{II}(NCMe)_6][B\{C_6H_3(CF_3)_2\}_4]_2$ with $[(Ph_3P)_2N]_2[Mn^{IV}(CN)_6]$ in THF/CH_2Cl_2 leads to the formation of dark green "$Fe[Mn(CN)_6]$", which is isomorphous with face-centered cubic Prussian blue [*Fm3m* space group, $a = 9.6$ (1) Å]. Based on the IR ν_{CN} absorption [2127 cm^{-1} (s), $\sim$2170 cm^{-1} (w,sh)], X-ray photoelectron spectroscopy (XPS; Fe $2p_{3/2}$ = 710.1 eV; Mn $2p_{3/2}$ = 641.8 eV), and ^{57}Fe Mössbauer spectroscopy [23% Fe^{II} (high spin), 72% Fe^{III} (high spin), 3% Fe^{II} (low spin), 2% Fe^{III} (low spin)] as well as charge neutrality, this material is formulated as $Fe^{II}_{0.23}Fe^{III}_{0.72}Mn^{III}_{0.02}Mn^{IV}_{0.03}[Mn^{IV}(CN)_6]_{0.23}[Mn^{III}(CN)_6]_{0.72}[Fe^{III}(CN)_6]_{0.02}[Fe^{II}(CN)_6]_{0.03}$ (**1**). This arises from a not understood combination of election transfer and linkage isomerization. This solid is stable in its anhydrous form, but quickly becomes deep blue ($\nu_{CN} = 2142\ cm^{-1}$) upon hydration to form $\{Fe^{II}_{0.15}Fe^{III}_{0.80}Mn^{III}_{0.01}Mn^{IV}_{0.04}[Mn^{IV}(CN)_6]_{0.15}[Mn^{III}(CN)_6]_{0.80}[Fe^{III}(CN)_6]_{0.01}[Fe^{II}(CN)_6]_{0.04}\} \cdot x\,H_2O$ (**2**) another complex combination of site occupancies, election transfer, and linkage isomerization with the subsequent appearance of a new ν_{CN} absorption (2065 cm^{-1}) and an XPS peak consistent with $[Fe^{II}(CN)_6]^{4-}$ (Fe $2p_{3/2}$ = 708.4 eV). After the hydrated material has been mildly heated the composition becomes the less complex $\{Fe^{III}_{0.94}Mn^{IV}_{0.06}[Mn^{III}(CN)_6]_{0.94}[Fe^{II}(CN)_6]_{0.06}\} \cdot x\,H_2O$ (**3**). The complex nature of the ion and charge distributions, with each metal ion existing in two different oxidation states in two different sites within the solid, is attributed to partial charge transfer and linkage isomerization, which presumably occurs to differing degrees at different defect sites and emphasizes the elaborate nature of the details of the materials based on the seemingly simple Prussian blue structure type. Magnetic susceptibility measurements of **1** and **3** give room temperature moments, μ_{eff}, that are consistent with the formulations [$\mu_{eff} = 6.51\ \mu_B$ (6.47 calcd) and $= 6.59\ \mu_B$ (6.40 calcd), respectively]. A Curie–Weiss constant, θ, of -8 K for **1** is consistent with the spin sites being antiferromagnetically coupled, and bulk ferrimagnetic order is observed below its T_c of 15.0 K. Compounds **2** and **3** are also magnetically ordered with T_c's of 18.7 and 10.1 K, respectively. Compounds **1**, **2**, and **3** each exhibit hysteresis with low coercive fields of 3, 1, and 4 Oe, respectively. These are surprising low values as **1**, **2**, and **3** possess significant crystallographic disorder as evidenced by X-ray diffraction studies and this results in spin-glass behavior in accord with the significant frequency dependence of the alternating current (ac) susceptibility data.

Keywords: electron transfer · ferrimagnet · iron · linkage isomerizations · manganese · prussian blue · spin glass

Introduction

The development of molecule-based magnets is a contemporary research area[1] with recent efforts focused on materials that possess bulk magnetic order near or above room temperature.[2–5] Mixed-metal hexacyanide systems possessing the Prussian blue face-centered cubic lattices represent one class of such materials.[3–5] Ideally, Prussian blue structured materials have $\cdots\rightarrow M \leftarrow C{\equiv}N \rightarrow M' \leftarrow N{\equiv}C \rightarrow M \cdots$ repeat units along all three crystallographic axes. The magnetic-coupling and -ordering temperatures can be varied through the use of different combinations of metals (M and M′) and/or their oxidation states.[3–5] Examples of compounds with the highest magnetic-ordering temperatures, T_c, include $Cr^{II}_{1.5}[Cr^{III}(CN)_6] \cdot 5\,H_2O$ ($T_c = 240$ K)[3b] and the room-temperature magnet $V[Cr(CN)_6]_{0.86} \cdot 2.8\,H_2O$ ($T_c = 315$ K).[4] The magnetic behavior is attributed to the strong antiferromagnetic coupling between adjacent metal sites through the antibonding orbitals of the bridging cyanide ligands.[3b, 4, 6] Most Prussian blue structured materials, including Prussian blue (Fe^{III}_4-

[a] Prof. J. S. Miller, Dr. W. E. Buschmann
Department of Chemistry, 315 S. 1400 E. RM Dock
University of Utah, Salt Lake City, UT 84112-0850 (USA)
Fax: (+1) 801-581-8433
E-mail: jsmiller@chemistry.utah.edu

[b] Prof. P. Gütlich, Dr. J. Ensling
Institut für Anorganische Chemie und Analytische Chemie
Johannes-Gutenberg Universität, D-55099 Mainz (Germany)
Fax: (+49) 6131-392373
E-mail: p.guetlich@uni-mainz.de

  0947-6539/99/0510-3019 $ 17.50+.50/0

$[Fe^{II}(CN)_6]_3$), itself a magnet with a T_c of 5.6 K,[7] have differing oxidation states and lack the ideal 1:1 M:M′ ratio; this results in defect-ridden structures.[7] When the sum of M and M′ oxidation states equals the coordination number, six, then, in principle, the structure should not have either cation or anion defects.

For Prussian blue structured materials ferromagnetic coupling and subsequently ferromagnetic order is achieved when spins on adjacent spin sites (M and M′) are in orthogonal orbitals as noted for $CsNi^{II}[Cr^{III}(CN)_6]$ ($T_c = 90$ K).[5] Here the d^8 Ni^{II} and d^3 Cr^{III} have the e_g^2 and t_{2g}^3 electronic configurations, respectively; hence they possess spins in adjacent orthogonal orbitals. To eliminate the need for an auxiliary cation as well as minimize structural defects and to maximize the ferromagnetic coupling, $Ni^{II}[Mn^{IV}(CN)_6]$ was targeted for preparation.[8] This required $[Mn^{IV}(CN)_6]^{2-}$, which was recently prepared from aprotic media.[9] In addition to the ferromagnetic coupling expected for $Ni^{II}[Mn^{IV}(CN)_6]$, $Fe^{II}[Mn^{IV}(CN)_6]$ with high-spin d^6 Fe^{II} ($t_{2g}^4e_g^2$) and d^3 Mn^{IV} (t_{2g}^3) should exhibit antiferromagnetic coupling and order as a ferrimagnet. Herein, we report the preparation and unexpected electron transfer and partial ligand isomerization of $Fe[Mn(CN)_6]$.

Results and Discussion

The reaction of $[(Ph_3P)_2N]_2[Mn^{IV}(CN)_6]$ and $[Fe^{II}(NCMe)_6][B\{C_6H_3(CF_3)_2\}_4]_2$ leads to the formation of insoluble, dark green, hydroscopic "$Fe[Mn(CN)_6]$" (**1**). In its simplest formulation this compound is valence-ambiguous as it can be formulated as either $Fe^{II}[Mn^{IV}(CN)_6]$ or $Fe^{III}[Mn^{III}(CN)_6]$, the latter requiring an electron transfer process. Although stable to oxidation from oxygen, it is unstable when exposed to moisture leading to an unstable hydrated species (**2**) that turns into a deep blue compound (**3**); these were characterized by IR, XPS, and Mössbauer data. Thermal treatment of **1** also forms **3**, but more slowly and with significant decomposition due to the elevated temperature (> 80 °C) required to promote the transformation.

Infrared analyses: The single, broad band of the ν_{CN} absorption of Prussian blue structured materials is diagnostic of the C-bound metal ion and its oxidation state, but is much less sensitive to the N-bound metal ion and its oxidation state. For example, the ν_{CN} values for $[PPN]_2[Mn^{IV}(CN)_6]$, $K_2[Mn^{IV}(CN)_6]$, $[PPN]_3[Mn^{III}(CN)_6]$, $K_3[Mn^{III}(CN)_6]$, $[PPN]_3[Fe^{III}(CN)_6]$, $K_3[Fe^{III}(CN)_6]$, and $K_4[Fe^{II}(CN)_6]$, are 2132,[9] 2150,[10] 2092 and 2098 cm^{-1},[11] 2112 and 2121,[12a] 2096,[13] 2115,[12a] and 2033 and 2021 cm^{-1} [12b] respectively. The ν_{CN} ranges for the N-bound Prussian blue lattice ions of $[Mn^{II}(CN)_6]^{4-}$, $[Mn^{III}(CN)_6]^{3-}$, and $[Mn^{IV}(CN)_6]^{2-}$ are 2060,[12a] 2125 – 2150,[14, 15] and 2155 – 2183 cm^{-1},[11, 16] respectively.

The IR spectrum of anhydrous **1** shows a broad (80 cm^{-1} FWHM) strong ν_{CN} absorption at 2127 cm^{-1}, Figure 1, in the range consistent with the formulated trivalent oxidation state of the $[Mn^{III}(CN)_6]^{3-}$ ion.[14, 15] (Compound **1** also exhibits a weak shoulder absorption at 2070 cm^{-1} assigned to a small amount of an unknown secondary phase.) Hence, based on-

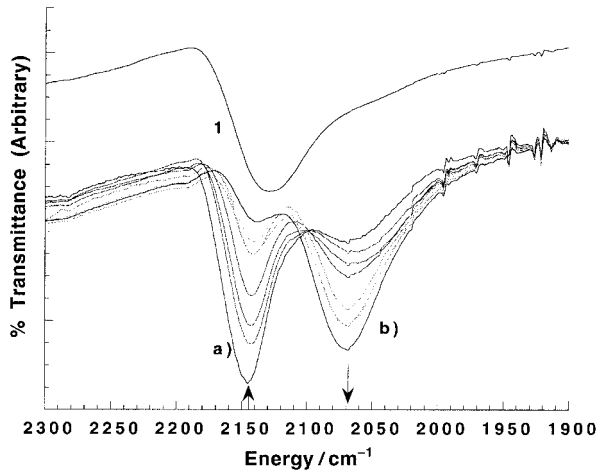

Figure 1. IR ν_{CN} spectra of anhydrous **1** (top), and **1** exposed to moisture then heated to 80 °C as a Nujol mull for 24 h. Peak a) $[Mn^{III}(CN)_6]^{3-}$ looses intensity, while peak b) $[Fe^{II}(CN)_6]^{4-}$ gains intensity. The first four spectra of the series are recorded in the first 2 h.

the ν_{CN} IR data, **1** is formulated as predominantly $Fe^{III}[Mn^{III}(CN)_6]$. However, the broad ν_{CN} absorption extends to ~2180 cm^{-1} (Figure 1) and does not eliminate the possibility of the presence of $[Mn^{IV}(CN)_6]^{2-}$. Trace amounts of THF are also evident in the IR with a weak, characteristic absorption between 1029 to 1034 cm^{-1}. THF, however, is quickly displaced by water upon exposure to moisture and the solid turns deep blue. The freshly prepared (anhydrous) compound is relatively stable at room temperature.

Upon heating, the ν_{CN} absorption band for anhydrous **1** changes from 2127 to ~2065 cm^{-1}. At temperatures needed to induce the transformation (ca. 80 °C) some decomposition leading to the growth of an additional absorption at 2205 cm^{-1} occurs. This thermally induced transformation is detected in the TG (thermal gravimetric) and DSC (differential scanning calorimetry) analyses, Figure 2. The onset of an endothermic

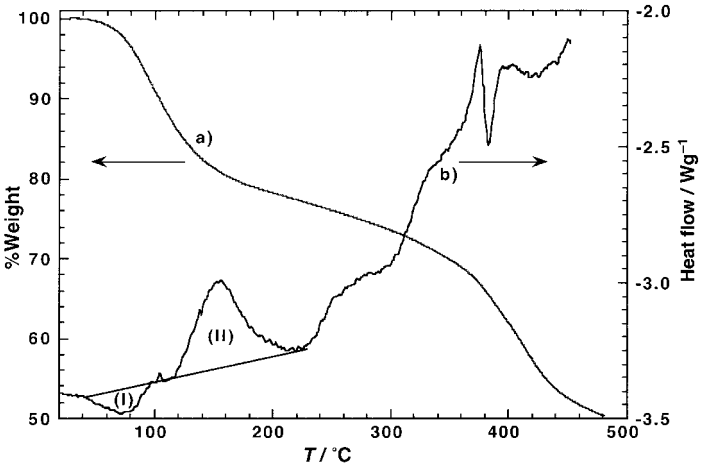

Figure 2. Thermal analyses of anhydrous $Fe[Mn(CN)_6]$; a) TGA and b) DSC curves. Energy of transition (I) is 6.0 kJ mol^{-1}, endothermic, and (II) is 27.7 kJ mol^{-1}, exothermic.

transition in the DSC occurs at about 45 °C followed by the onset of an exotherm at 118 °C. The exotherm is accompanied by a significant weight loss shown in the TGA curve that is

0947-6539/99/0510-3020 $ 17.50+.50/0 *Chem. Eur. J.* **1999**, *5*, No. 10

due to loss of cyanide radicals in the form of cyanogen, as observed by TGA/mass spectrometry. The irreversible endothermic transition is not accompanied by a weight loss event and is, therefore, assigned to an irreversible structural transformation. The 2205 cm^{-1} ν_{CN} absorption band and observation of cyanogen in the mass spectra suggest the formation of $[Mn^{II}(CN)_4]^{2-}$ by the thermolysis of $[Mn^{IV}(CN)_6]^{2-}$.[17]

Upon exposure of **1** to moisture, **2** forms with a concomitant shift in the ν_{CN} absorption from 2127 cm^{-1} to 2142 cm^{-1} and new absorptions at 3400 and 1660 cm^{-1} assigned to the presence of water. This shift occurs in the presence and absence of oxygen. After this shift has occurred, the 2142 cm^{-1} absorption loses intensity and a new absorption grows in at 2065 cm^{-1} at room temperature, indicating the formation **3**. These transformations are also insensitive to the presence of oxygen, but are accelerated by heating (Figure 1). They are very rapid at first and then slow down as the reaction proceeds. Finally, these transformations can be accelerated by heating ($>80\,^{\circ}C$), but cannot be pushed to 100% completion owing to concomitant decomposition.

The appearance of the 2142 cm^{-1} ν_{CN} absorption is attributed to hydration, since the absorption frequency still lies within the range found for N-bound $[Mn^{III}(CN)_6]^{3-}$.[14, 15] The increase from 2127 to 2142 cm^{-1} is consistent with a decrease in the Fe–NC π-back-bonding interaction. This is consistent with the N-bound Fe^{II} cation being oxidized to Fe^{III}; this involves decreasing the π-back-bonding and strengthening the CN bond, which leads to a shift to higher frequency of the ν_{CN} vibration. The second lower frequency 2065 cm^{-1} ν_{CN} absorption resulting from hydration is consistent with $[Fe^{II}(CN)_6]^{4-}$[18] and not $[Fe^{III}(CN)_6]^{3-}$, which is typically around 2165 cm^{-1}.[18b, 19]

Based on the ν_{CN} absorptions, compound **3** is formulated as predominantly $Mn^{IV}[Fe^{II}(CN)_6]$ with some residual $Fe^{III}[Mn^{III}(CN)_6]$ present.[22] Hence, some linkage isomerization of CN ligand as well as an electron transfer between ions occurs. Linkage isomerization has also been observed for $Fe^{II}_3[Mn^{III}(CN)_6]_2 \cdot x\,H_2O$[19, 20] as well as related Fe–Cr,[19, 21] and Cr–Co[19, 20] systems made in aqueous media.

X-ray diffraction: The observed reflections in the powder X-ray diffraction patterns are very broad, but regions of diffraction intensity are consistent with the most intense diffraction peaks expected for a face-centered cubic Prussian blue type structure, Figure 3. The poor quality of both powder patterns limits the accuracy of the determination of the lattice constant, *a*, from the *d*-spacing of the low-angle diffraction-peak maximum. For **1** *a* is 9.6 (1) Å. This is shorter than typical values of *a* for the Prussian blue analogues, which range from 10.1 to 10.8 Å.[7, 23–25] The lower value of *a* is likely to be due to a contraction of the lattice in the absence of water that is necessary to help stabilize the structure during lattice formation. This is observed in a structural study of $Mn_3[Co(CN)_6]_2 \cdot 12\,H_2O$ which revealed that hydrogen bonding of zeolitic water plays a major role in stabilizing the face-centered cubic lattice, that *a* decreases from 10.44 to 10.22 Å, and that the diffraction peaks become very diffuse upon dehydration.[25a] The presence of empty cavities within a Prussian blue structural framework leads to an unstable state

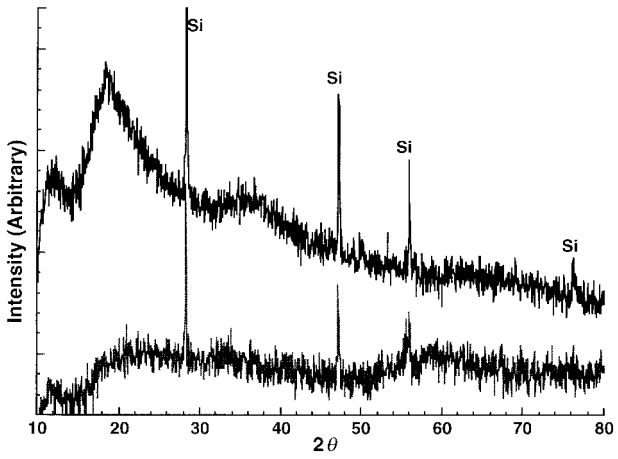

Figure 3. Powder X-ray diffraction patterns of anhydrous $Fe[Mn(CN)_6]$ (**1**, top) and after hydration and isomerization to $Mn[Fe(CN)_6]$ (**3**, bottom). Silicon was used as an internal standard.

relative to the entropy gained upon filling that space.[26] For the nonaqueously prepared compounds studied herein, the ordered Prussian blue type lattices are inherently unstable with the vacant pore space; this results in significant crystallographic disorder. The presence of lattice disorder is also supported by ac-susceptibility studies, vide infra.

The broadening of the X-ray diffraction peaks can be related not only to the degree of crystallinity, but also to the crystallite size. From the Scherrer formula,[27] the estimated particle size for **1** is unreasonably small, about 17 Å. Particles approximately one to two unit cells in size are far too small to have long-range magnetic interactions (vide infra), as is the case for superparamagnets;[28] this renders the observed bulk magnetic ordering an impossibility. The broadening of the X-ray diffraction peaks is, therefore, attributed to a significant contribution from lattice disorder and a less dramatic reduction in particle size.

X-ray photoelectron spectroscopy (XPS): The oxidation states of the two metal centers in **1** and **3** were independently determined by XPS. The observed Fe $2p_{3/2}$ electron binding energy of anhydrous "$Fe^{III}[Mn^{III}(CN)_6]$" (**1**) is 710.1 eV and the Mn $2p_{3/2}$ binding energy is 641.8 eV, Table 1. Standard compounds, $K_3[Mn^{III}(CN)_6]$, $[(Ph_3P)_2N]_3[Mn^{III}(CN)_6]$, and $[(Ph_3P)_2N]_2[Mn^{IV}(CN)_6]$ (Table 1) were analyzed to confirm

Table 1. XPS of $Fe[Mn(CN)_6]$ compared with the hexacyanomanganates.

Compound[a]	Binding energy [eV][b]				
	N	Anion, $[M(CN)_6]^{n-}$		Cation	
	1s	$2p_{1/2}$	$2p_{3/2}$	$2p_{1/2}$	$2p_{3/2}$
$K_4[Fe^{II}(CN)_6]$[29]	398.0	[c]	708.4 (Fe^{II})	[c]	291.9 (K^+)
$K_3[Fe^{III}(CN)_6]$[29]	398.1	[c]	710.1 (Fe^{III})	[c]	291.9 (K^+)
$K_3[Mn^{III}(CN)_6]$	397.6	653.5	641.6 (Mn^{III})	294.7	292.6 (K^+)
$(PPN)_3[Mn^{III}(CN)_6]$	397.2	652.6	640.6 (Mn^{III})	132.7 (P 2p)	
$(PPN)_2[Mn^{IV}(CN)_6]$	398.2	654.5	642.8 (Mn^{IV})	133.2 (P 2p)	
1	398.0	653.4	641.8 ($Mn^{III/IV}$)	723.8	710.1 (Fe^{III})
2	398.2	653.6	641.7 ($Mn^{III/IV}$)	724.5	711.0 (Fe^{III})
3	397.9	652.3	640.4 (Mn^{III})	723.8	710.4 (Fe^{III})
		721.1	708.4 (Fe^{II})		

[a] Compounds were mounted as powders on double-sided conducting tape. [b] Spectra were normalized on the C 1s peak at 284.6 eV. [c] Not reported.

the relative binding energies as a function of oxidation state. The transformation of **1** to **2** does not significantly change the Mn $2p_{3/2}$ binding energy, but there is a 1.3 eV decrease in binding energy to 640.4 eV upon transformation to **3**; this shows that there is a significant change in oxidation state and/or ligand-field environment.

Differences in oxidation states are more easily resolved for Fe and the observed $2p_{3/2}$ electron binding energy, 710.1 eV, is consistent with the values of 710.1 and 709.6 eV reported for $K_3[Fe^{III}(CN)_6]$.[29] There is a 0.9 eV increase in the Fe $2p_{3/2}$ binding energy upon hydration of **1**, while the Mn $2p_{3/2}$ binding energy remains constant at 641.7 eV. The spectrum of **3** (ca. 75% transformed by IR) shows two resolved $2p_{3/2}$ peaks for Fe (708.4 eV, Fe^{II} and 710.4 eV, Fe^{III}), while the Mn $2p_{3/2}$ binding energy decreases to 640.4 eV. Previous studies report the Fe $2p_{3/2}$ binding energy in $K_4[Fe^{II}(CN)_6]$ to be in the range 707.1 – 708.5 eV.[29] These results are qualitatively consistent with the IR studies and confirm that Fe^{II} is converted to Fe^{III} and that Mn^{IV} is converted to Mn^{III}. The data are not consistent, however, with the formation of Mn^{IV}-$[Fe^{II}(CN)_6]$.

Table 2. Summary of the ^{57}Fe Mössbauer and magnetic properties for **1**, **2**, and **3**.

	1	**2**	**3**
Isomer shift δ [mm s^{-1}]	0.56, 0.46, 1.21	0.48, 0.47, 1.16	0.49, 0.28
Quadrupole splitting, ΔE, [mm s^{-1}]	1.01, 0.76, 2.91	0.80, 0.76, 2.97	0.90, 0.81
Internal field [kOe] (1.9 K)	54.6		
Effective Curie – Weiss const θ' [K]			
$50 < T < 150$ K	30	25	– 25
Critical temperature T_c [K]			
[from $M(T)$]	22	19	19
[from the peak in $\chi'(T)$]	15.0	13.1	10.1
"Glassiness" figure of merit ϕ	0.017	0.026	0.039
Magnetization at 50 kOe [emu Oe mol^{-1}]	21600	21600	13300
Coercive field H_{cr} [Oe]	3	1	4

Mössbauer spectroscopy: Temperature-dependent ^{57}Fe Mössbauer spectra for **1** were recorded below 20 K (Figure 4 left). These spectra reveal the onset of magnetic ordering below

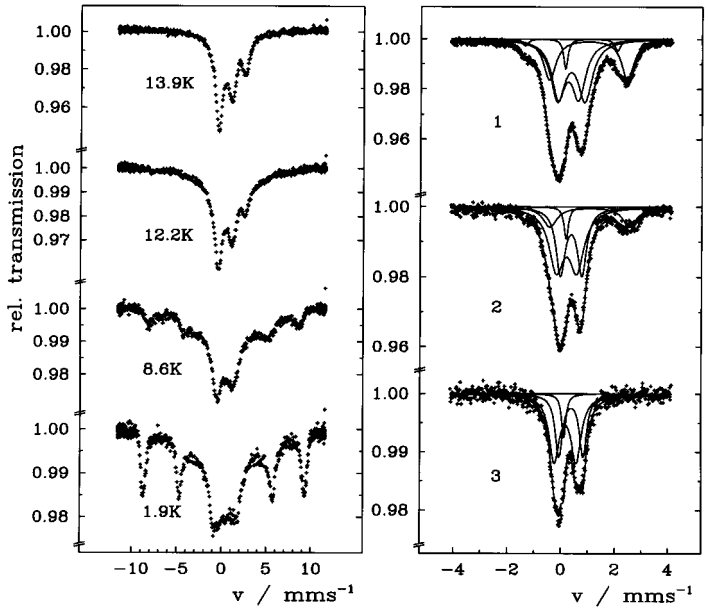

Figure 4. ^{57}Fe Mössbauer spectra for **1** below 20 K (left) and as a function of hydration for **1**, **2**, and **3** at 130 K (right).

~14 K. Even at 1.9 K the magnetic splitting of the high-spin ferric components is not completely developed, as a broad, intense background is present that screens unresolved magnetically split components of both high-spin Fe^{III} and Fe^{II}. The magnetic hyperfine field of the sextet component of 54.6 T is typical for high-spin Fe^{III}.[30] This feature of the Mössbauer spectra in the magnetically ordered phase (below the transition temperature) is indicative of the spin-glass property of sample **1**; this is also realized by the frequency dependence of $\chi'(T)$ and $\chi''(T)$ (see below).

The 130 K ^{57}Fe Mössbauer data taken on two independently prepared samples are very similar to one another (Figure 4 (right), Table 2) and can be understood from the related model compounds.[30] For the anhydrous **1**, 72 ± 2% of the relative area is attributed to a broad doublet assigned to high-spin, N-bound Fe^{III} (Table 2). This broad doublet was resolved into two doublets at $\delta = 0.56$ mm s^{-1} ($\Delta E = 1.01$ mm s^{-1}) and $\delta = 0.46$ mm s^{-1} ($\Delta E = 0.76$ mm s^{-1}), which suggests two high-spin Fe^{III} sites, as typical N-bound high-spin Fe^{III} has $\delta = 0.49$ mm s^{-1} ($\Delta E = 0.57$ mm s^{-1}).[30, 31a] These two Fe^{III} sites can be attributed to a distribution of Fe sites with a full octahedral *N*-coordination sphere ($\Delta E = 0.76$ mm s^{-1}) and to a less than octahedral (i.e., lower symmetry) coordination sphere ($\Delta E = 1.01$ mm s^{-1}) due to structural defects/vacancies. The second major component of the spectrum is a doublet of 23 ± 1% relative area for high-spin, N-bound Fe^{II} at $\delta = 1.21$ mm s^{-1} ($\Delta E = 2.91$ mm s^{-1}) [cf. typical N-bound high-spin Fe^{II} have $\delta = 0.98$ mm s^{-1} ($\Delta E = 2.67$ mm s^{-1})[29, 31b]]. The remaining 5% area is fit to peaks that correspond to low-spin, C-bound Fe^{III} (2 ± 1%) and low-spin, C-bound Fe^{II} (3 ± 1%). These results in concert with the IR and XPS data as well as charge neutrality suggest that the initial product formed undergoes only a partial electron transfer resulting in a composition of $Fe^{II}_{0.23\pm0.01}Fe^{III}_{0.72\pm0.02}$-$Mn^{III}_{0.03\pm0.01}Mn^{IV}_{0.02\pm0.01}[Mn^{IV}(CN)_6]_{0.23\pm0.01}[Mn^{III}(CN)_6]_{0.72\pm0.02}$-$[Fe^{III}(CN)_6]_{0.02\pm0.01}[Fe^{II}(CN)_6]_{0.03\pm0.01}$, **1**, with ~5% linkage isomerization.[22] The Mn^{III}/Mn^{IV} ratio is assumed to follow the Fe^{II}/Fe^{III} ratio in that when a Fe^{II} site is oxidized, a Mn^{IV} center is reduced because the transformation is not influenced by the presence of oxygen (vide supra).[32] The fractional electron transfer and partial linkage isomerization maybe due to the type and quantity of defect sites, with different types of defects stabilizing electron transfer and linkage isomerization to different extents. Evidently, as a result of the complexity of the site occupancy distribution of the different ions in different oxidation states, the determination of their ratios are problematic. Nonetheless, even with errors associated with each fractional occupancy, it is clear that Mn^{III}, Mn^{IV}, Fe^{II},

0947-6539/99/0510-3022 $ 17.50+.50/0 *Chem. Eur. J.* **1999**, *5*, No. 10

and Fe^{III} are bound to both C and N, until **3** is formed (vide infra).

Hydration of **1**, by exposure to wet methanol to form **2**, led to an increase in the relative area for high-spin Fe^{III} accompanied by a decrease in the amount of high-spin Fe^{II}. This results in a composition of approximately $\{Fe^{II}_{0.15\pm0.01}Fe^{III}_{0.80\pm0.02}Mn^{III}_{0.01\pm0.01}Mn^{IV}_{0.04\pm0.01}[Mn^{IV}(CN)_6]_{0.15\pm0.01}[Mn^{III}(CN)_6]_{0.80\pm0.02}[Fe^{III}(CN)_6]_{0.01\pm0.01}[Fe^{II}(CN)_6]_{0.04\pm0.01}\}\cdot x\,H_2O$ for **2**. There is no concomitant increase in the total relative amount of low-spin Fe ions, which suggests that linkage isomerization does not occur in this hydration process.

Heating **2** to 40 °C for 4 h (below its decomposition temperature) increases the relative area for high-spin Fe^{III} to 94%, eliminates high-spin Fe^{II}, and only about 5% low-spin Fe^{II} remains. Furthermore, there is no evidence for an Fe^{III}-oxyhydroxy species ($\delta = 0.63$ mm s^{-1}, $\Delta E = 0.58$ mm s^{-1}).[19, 20b] Therefore, all the Fe sites detected are C- or N-bound. This shows that the final composition of $\{Fe^{III}_{0.94\pm0.02}Mn^{IV}_{0.06\pm0.01}[Mn^{III}(CN)_6]_{0.94\pm0.02}[Fe^{II}(CN)_6]_{0.06\pm0.01}\}\cdot x\,H_2O$ for **3** is stable and only has one oxidation state for each metal ion bound to C or N of the cyanide group.

In general, the results of the Mössbauer studies show that the initially formed "$Fe^{II}[Mn^{IV}(CN)_6]$" undergoes a partial, irreversible electron transfer to form **1**. The electron transfer can be driven to completion by hydrating the lattice through an unstable intermediate, **2**, that slowly transforms to **3**. A small portion (ca. 5%) of the material undergoes a linkage isomerization upon formation, but does not continue to isomerize after isolation. The presence of this as either a mixed or separate phase cannot be determined by these studies.

The results of the IR and XPS studies are in qualitative agreement with one another as to the nature of the ionic units that comprise the Prussian blue lattice and suggest that this material undergoes electron transfer between metal ions as well as linkage isomerization of the bridging cyanide ligands. This is reasonable since electron transfer (e.g., Turnbull's blue,[33] mangano-manganicyanide[16]) and linkage isomerization (e.g., $Fe^{II}_3[Mn^{III}(CN)_6]_2\cdot x\,H_2O$)[19, 20] are known to occur in some Prussian blue structured materials.

More sensitive Mössbauer studies, however, suggest that electron transfer accounts for about 95% of the material's behavior and that there is very little (ca. 5%) linkage isomerization. This result is reasonable, but creates a discrepancy between the interpretation of IR/XPS and Mössbauer results—the most heavily relied upon techniques used for analysis of Prussian blue analogues.[12, 19–21, 29, 31a, 33–35] This raises some important questions as to what is actually occurring in these materials and what is observed in the IR.

The following observations are important for addressing this discrepancy. First, an electron transfer event between metal ions is consistent with all of the spectroscopic data to give the Fe^{III}–Mn^{III} oxidation states as the major component of **1**. Second, a linkage isomerization of the cyanide ligands resulting in a low-spin $[Fe^{II}(CN)_6]^{4-}$ ion appears to occur after hydration of **1** according to IR. According to Mössbauer this linkage isomerization occurs only during the initial product formation and accounts for only up to 6% of the material. Third, analysis between the IR and Mössbauer data for **2** and **3** have the greatest discrepancy. The IR ν_{CN} absorptions correspond to $[Mn^{III}(CN)_6]^{3-}$ (2127 cm^{-1}) initially and ~75% conversion to $[Fe^{II}(CN)_6]^{4-}$ (2065 cm^{-1}) through hydration and heating (Figure 1). In contrast, the Mössbauer data (Figure 4) indicate that ~94% of the material undergoes electron transfer to give $Fe^{III}[Mn^{III}(CN)_6]$ as the final product, but the ν_{CN} absorption for this is expected to fall between 2125 and 2150 cm^{-1}.[14, 15]

The area of the 2065 cm^{-1} absorption for **3** relative to the areas of the 2127 and 2142 cm^{-1} absorptions for **1** and **2** is unexpectedly similar assuming that electron transfer accounts for 94% of the material. The oscillator strengths of the hexacyano complexes decrease with increasing atomic number and oxidation state.[34c] The ν_{CN} oscillator strengths for $K_3[Mn^{III}(CN)_6]$, $K_3[Fe^{III}(CN)_6]$, and $K_4[Fe^{II}(CN)_6]$ are reported to be 8200, 12300, and 92000 mol^{-1}cm^{-1}, respectively.[34c] In **1** the $[Mn^{III}(CN)_6]^{3-}$ and $[Fe^{III}(CN)_6]^{3-}$ peaks overlap and appear as one broad absorption; however, the presence of $[Fe^{II}(CN)_6]^{4-}$ is resolved. Based on the oscillator-strengths, $[Fe^{II}(CN)_6]^{4-}$ should exhibit a ν_{CN} absorption approximately 11 times greater than that of the $[Mn^{III}(CN)_6]^{3-}$ ion. For the 6% $[Fe^{II}(CN)_6]^{4-}$ present in **3** the expected $[Mn^{III}(CN)_6]^{3-}$:$[Fe^{II}(CN)_6]^{4-}$ ratio is ~1.4:1. This does not fully account for the greater area of the 2066 cm^{-1} absorption. There are no trivalent hexacyanoferrate or manganate species in a Prussian blue material known to have their primary intense ν_{CN} absorption below 2100 cm^{-1},[13, 14, 34a] therefore, the 2066 cm^{-1} absorption can only be due to $[Fe^{II}(CN)_6]^{4-}$,[32] and the oscillator strength of this ion in a Prussian blue lattice is likely greater than the potassium salt predicts.

Magnetic susceptibility: The 2–300 K magnetic susceptibility (χ) of **1**, **2**,[36] and **3** were measured by cooling to 2 K in zero field and measuring in a 5 Oe field upon warming, and were fit to the Curie–Weiss law, $\chi \propto (T-\theta)^{-1}$ (Figure 5). For **1** θ is

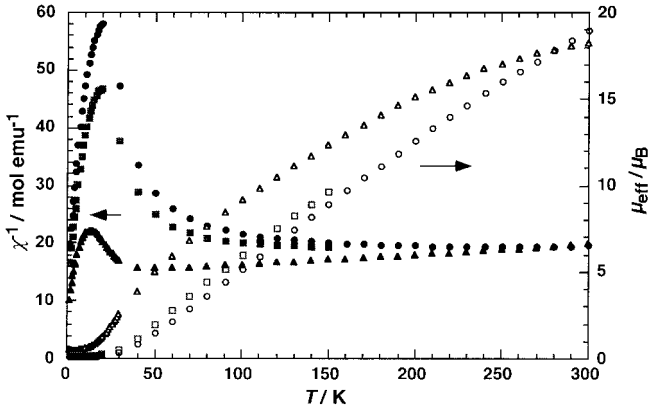

Figure 5. Temperature-dependent $1/\chi$ and μ_{eff} curves for **1** (○, ●), **2** (□, ■), and **3** (△, ▲).

−8 K for data taken above 200 K and ~30 K for $50 < T < 150$ K. For **2** θ is 25 K for $50 < T < 150$ K; data above 150 K was avoided owing to its facile transformation to **3**. In contrast, **3** does not obey Curie–Weiss law as it has a very nonlinear behavior, which leads to unreliable values for θ. For comparison, however, the θ above 200 K is about −500 K,

while for $50 < T < 150$ K it is about -25 K. The negative θ values are indicative of antiferromagnetic coupling, which is consistent with the expected exchange.[1c, 23, 24, 28] At lower temperature ferromagnetic coupling ($\theta > 0$) is evident.

The 300 K effective moment [$\mu_{eff} \equiv (8\chi T)^{1/2}$] for **1** is 6.51 μ_B, (Figure 5). This is consistent with the calculated spin-only value of 6.47 μ_B assuming $g = 2$. Compound **2** was measured only up to 150 K to avoid further transformation (Figure 5), but its μ_{eff} converges with the data for **1**. Compound **3** has a μ_{eff} of 5.18 μ_B at 50 K and increases to 6.59 μ_B at 300 K (Figure 5), which is slightly higher than the calculated spin-only value of 6.40 μ_B. Significant contributions from spin-orbit coupling due to high-spin $S = 2$ Fe^{II} and low-spin $S = 1$ $[Mn^{III}(CN)_6]^{3-}$ are not included in the simple approximations of μ_{eff} and are known to increase the values significantly.[11, 37, 38] The measured μ_{eff} are in good agreement with the assignments made from the Mössbauer data.

The magnetization as a function of temperature, $M(T)$, shows a dramatic increase below 22 K for **1** and below 19 K for both **2** and **3** (Figure 6). This behavior is indicative of

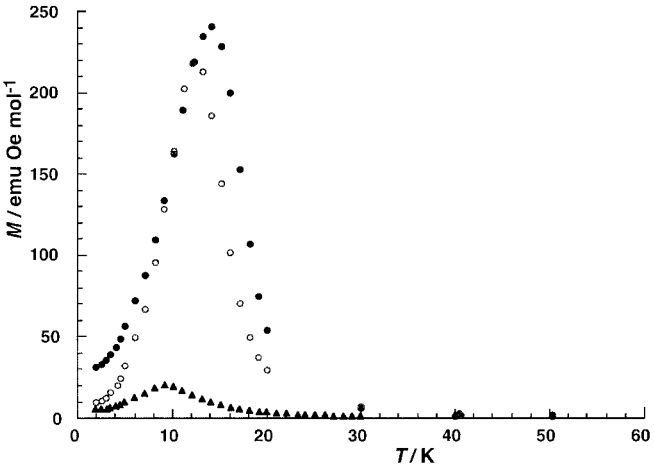

Figure 6. Low-field, temperature-dependent magnetization curves (M vs. T) for **1** (●), **2** (○), and **3** (▲).

spontaneous bulk magnetic ordering and the values of 22 and 19 K can be used to approximate the critical temperatures, T_c. These values are determined by extrapolating the steepest slope of the magnetization curve to the temperature axis of $M(T)$ plots. This is additional evidence for the two forms being essentially the same as formulated. The magnitude of the magnetization maximum below T_c, however, drops from ~ 240 emu Oe mol^{-1} for **1** to ~ 212 emu Oe mol^{-1} for **2** and then to ~ 19 emu Oe mol^{-1} for **3**, although **3** has nearly the same T_c as **2**. The differences in magnetization magnitude could be due to the presence of an increasing amount of diamagnetic $[Fe^{II}(CN)_6]^{2-}$ in the samples. The $[Fe^{II}(CN)_6]^{2-}$ content doubles from **1** (3%) to **3** (6%) and this increase in diamagnetic content should lead to a reduction in the nearest-neighbor interactions and, thus, a reduction in T_c (according to mean-field theory)[1c, 28, 39] and in the magnitude of the magnetization in the ordered state. This point is better resolved in the more sensitive ac-susceptibility measurements described below that are consistent with this assessment. A striking feature of the low-field $M(T)$ data (Figure 6) is that the magnetization increases with decreasing temperature through a maximum and drops to nearly zero at lower temperatures. This behavior may arise from a transition from a ferrimagnetically ordered state, below T_c, to a metamagnetic state as the temperature is lowered as observed for several [manganoporphyrin][TCNE]-based magnets.[40] Field-dependent magnetization measurements presented below support this possibility.

The temperature dependence of the ac-susceptibility measurements of **1** show both in-phase, χ' (absorptive), and out-of-phase, χ'' (dispersive), components of the susceptibility (Figure 7a). Measurements were made by cooling the compound

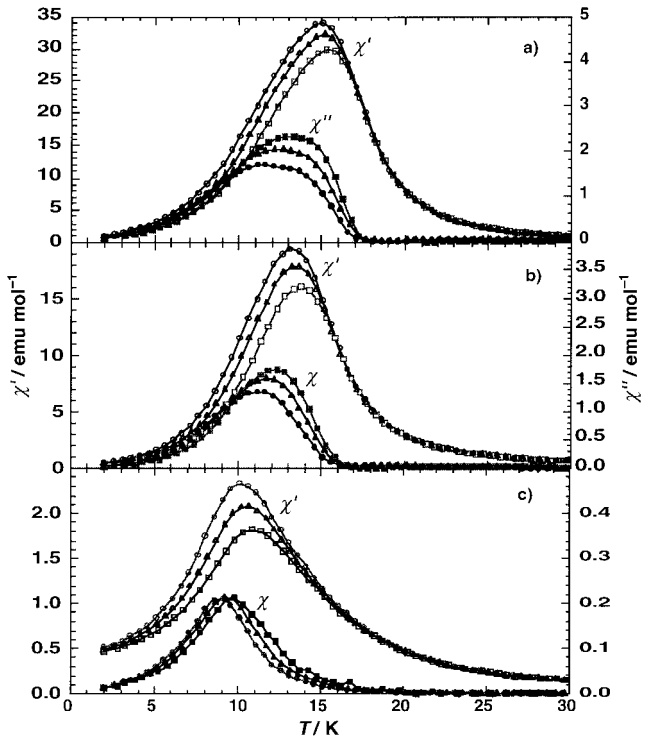

Figure 7. Temperature-dependent χ' and χ'' at 10 Hz (○, ●), 100 Hz (△, ▲), and 1000 Hz (□, ■) for a) **1**, b) **2**, and c) **3**. The samples were cooled in zero field to 2 K and data were measured upon warming with a 1 Oe ac field in a zero-applied dc field.

in zero field and measuring upon warming with a 1 Oe ac amplitude at driving frequencies of 10, 100, and 1000 Hz with zero-applied dc (direct current) field. The observance of χ'' is due to long-range magnetic order and an uncompensated moment, and, consequently, coercive behavior is expected. The T_c is best determined by the $\chi'(T)$ peak maximum at the lowest frequency, 10 Hz, closest to the zero-field dc limit. By this method the T_c for **1** is 15.0 K. There is evidence of a shoulder on the low-temperature side of the $\chi'(T)$ peak maximum for a secondary transition. The $\chi''(T)$ peak is also consistent with two overlapping transitions that make it unusually broad. The second transition contributing to the extra broadness of the $\chi'(T)$ and $\chi''(T)$ peaks is possibly due to a small amount of a secondary phase; this is consistent with the mixed composition determined for **1**. An independent secondary phase, however, that includes $[Fe^{II}(CN)_6]^{2-}$ should

0947-6539/99/0510-3024 $ 17.50+.50/0 *Chem. Eur. J.* **1999**, *5*, No. 10

have a greatly reduced T_c like that for Prussian blue[7] and be clearly resolved or nonordering and, therefore, not a contributor to the ac (alternating current) susceptibility. The ac-susceptibility data for **2** and **3** also have $\chi'(T)$ and $\chi''(T)$ components very similar to those of **1** (Figures 7b and 7c). The T_c, determined by the 10 Hz $\chi'(T)$ peak maximum is 13.1 K for **2**, and 10.1 K for **3**. These peaks appear to be representative of only one magnetic phase, although they are still relatively broad. The magnitude of the χ'(10 Hz) peaks for **1**, **2**, and **3** are about 34.1, 19.5, and 2.3 emu mol^{-1}, respectively, and are similar in relative magnitudes to the $M(T)$ values measured at 5 Oe. The concomitant decrease in T_c and magnitude of the $\chi'(T)$ peak maximum accompanying an increase in $[Fe^{II}(CN)_6]^{2-}$ content from **1** to **3** is consistent with the expectation that an increase in diamagnetic $[Fe^{II}(CN)_6]^{2-}$ content will reduce these quantities.

Frequency dependence in the $\chi'(T)$ and $\chi''(T)$ data around T_c is seen for all three samples. The shift in the peak maximum in χ' with frequency accompanied by a frequency-dependent χ'' component is indicative of spin-glass behavior.[41, 42] Spin-glass behavior results from contributions of randomness (i.e., site disorder, bond disorder, etc.) and mixed interactions (i.e., ferro- and antiferromagnetic coupling) within a material.[41a] The combination of randomness and competing ferro- and antiferromagnetic couplings between nearest-neighbor spin sites leads to spin frustration.[42] For each of these compounds the dominating contribution to spin-glass behavior is assumed to be from the crystallographic disorder, as evidenced from the broad reflections in the powder X-ray diffraction experiments (Figure 3). In these compounds, the T_c and T_f (spin-glass "freezing" temperature) occur at approximately the same temperature, giving rise to a single, albeit broad, frequency-dependent peak in both the $\chi'(T)$ and $\chi''(T)$.

Disorder resulting in glassiness appears as an increase in the frequency shift in T_f of the temperature at which χ'(10, 100, 1000 Hz) reaches a maximum. The frequency shift in T_f can also be used as a criterion to distinguish between different categories of materials exhibiting spin-glass behavior.[41b] The frequency shift is obtained from $\Delta T_f/T_f$ per decade frequency (ω) in Equation (1).

$$\phi = \Delta T_f/[(T_f \Delta(\log\omega)] \quad (1)$$

Use of the 10 and 1000 Hz data gives a ϕ of 0.017 for **1**, where $\Delta T_f = 0.5$, and T_f is the temperature at which χ'(10 Hz) has a peak. This value is consistent with an insulating spin glass.[41b] A comparable ϕ of 0.026 was obtained for **2**. This is not a significant change from the anhydrous compound and is consistent with the proposed hydration of the lattice without major structural changes. As the electron transfer is completed to give **3** there is still not a significant difference in ϕ (0.039). All nearest-neighbor interactions for **1**, **2**, and **3**, are expected to be antiferromagnetic as spins in adjacent spin sites do not reside in orthogonal orbitals. This is not strictly the case, however, since spin frustration must be present to give the spin-glass behavior observed. Therefore, the structural disorder in these compounds leads to some nearest-neighbor ferromagnetic interactions and spin frustration.

The field-dependent magnetization, $M(H)$, was measured at 5 K between $\pm$20 kOe after cooling in zero field. Hysteresis with weak coercive behavior is observed for **1**, **2**, and **3** with comparable coercive fields (H_c) of 3, 1, and 4 Oe, respectively (Figure 8). The initial rise in $M(H)$ lies outside the hysteresis

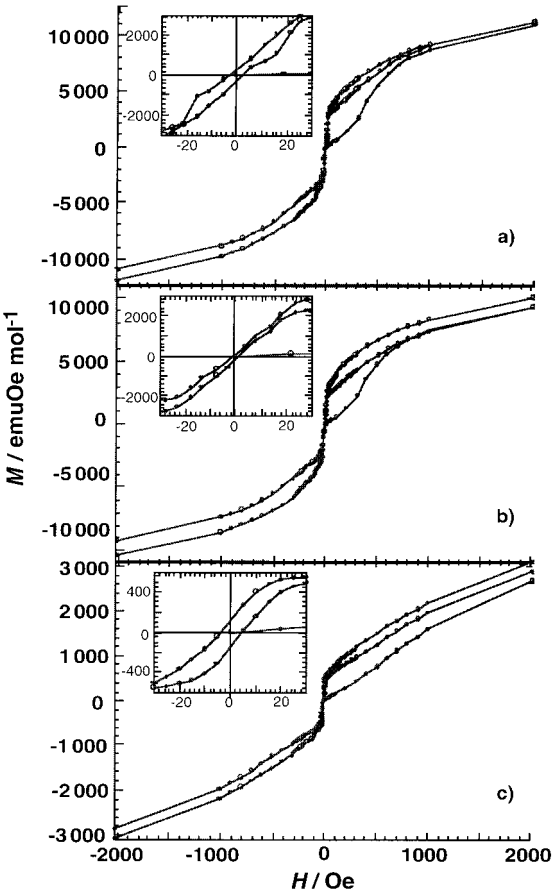

Figure 8. 5 K hysteresis curves for [magnetization (M) vs. applied magnetic field (H)] a) **1**, b) **2**, and c) **3**. Coercivity is shown in the inset. The samples were cooled in zero field to 5 K.

loops in each of the three samples and converges with the hysteresis curves above 1 kOe. The hysteresis curves are symmetric "S"-shaped about the zero point and they are all constricted. Constricted hysteresis is also a characteristic of materials with spin-glass behavior.[41b] The "S"-shaped initial magnetization curves are consistent with metamagnetic behavior[1c] and the critical fields at 5 K are relatively small, that is, $<$1000 Oe.

The 5 K $M(H)$ saturation curves of **1** and **2** have steep initial slopes below 2000 Oe, while the data for **3** increases at a much slower rate (Figure 9). Neither **1**, **2**, or **3** fully saturates at 50 kOe. The maximum observed saturation magnetizations (M_s) for **1** and **2** at 50 kOe are 21 600 emu Oe mol^{-1}, and are consistent with both having the similar electronic/spin structures. The observed M_s value for **3** is 13 300 emu Oe mol^{-1} at 50 kOe. Compounds **1**, **2**, and **3** do not reach full saturation and this behavior is likely to be related to the spin-glass behavior as well as the amount of spin, type of coupling, effective Landé g values, and anisotropy in the compounds.

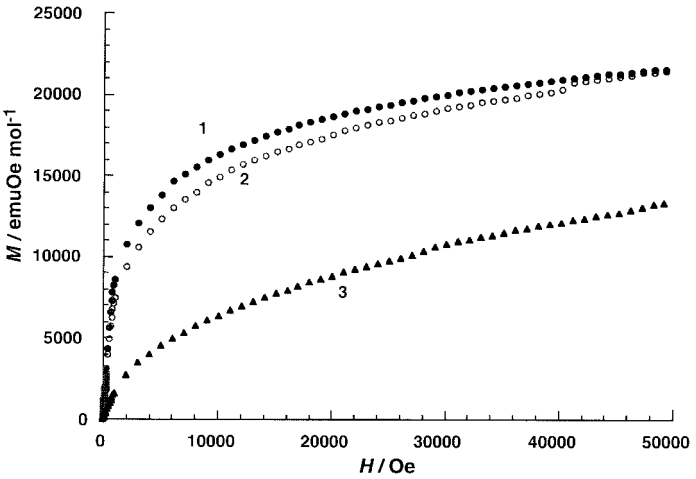

Figure 9. Field-dependent magnetization curves (M vs. H) for **1** (●), **2** (○), and **3** (▲). The samples were cooled in zero field to 5 K.

Conclusion

The reaction of Fe^{2+} with $[Mn^{IV}(CN)_6]^{4-}$, for which the formation of $Fe^{II}[Mn^{IV}(CN)_6]$ or perhaps its redox isomer $Fe^{III}[Mn^{III}(CN)_6]$ is anticipated, forms an anhydrous stable Prussian blue structured solid of composition $Fe^{II}_{0.23}Fe^{III}_{0.72}Mn^{III}_{0.02}Mn^{IV}_{0.03}[Mn^{IV}(CN)_6]_{0.23}[Mn^{III}(CN)_6]_{0.72}[Fe^{III}(CN)_6]_{0.02}[Fe^{II}(CN)_6]_{0.03}$ (**1**); this was elucidated from data acquired by techniques that include ^{57}Fe Mössbauer and IR spectroscpy, and XPS studies, and a consideration of charge neutrality. The changes in oxidation, spin, and isomerization states, and the extinction coefficients associated with species are all lumped into two broad ν_{CN} IR bands. These differences, however, are more reliably resolved with the Mössbauer data. The complex nature of the ion and charge distributions is attributed to partial local charge transfer and linkage isomerization that presumably occurs to differing degrees at different defect sites and emphasizes the elaborate nature of the details of the materials based on the seemingly simple Prussian blue structure type. Compound **1** is stable, but can be hydrated to form $\{Fe^{II}_{0.15}Fe^{III}_{0.80}Mn^{III}_{0.01}Mn^{IV}_{0.04}[Mn^{IV}(CN)_6]_{0.15}[Mn^{III}(CN)_6]_{0.80}[Fe^{III}(CN)_6]_{0.01}[Fe^{II}(CN)_6]_{0.04}\}\cdot x\,H_2O$ (**2**) as an unstable intermediate that transforms through an irreversible electron transfer between metal ions to $\{Fe^{III}_{0.94}Mn^{IV}_{0.06}[Mn^{III}(CN)_6]_{0.94}[Fe^{II}(CN)_6]_{0.06}\}\cdot x\,H_2O$ (**3**), which has only one oxidation state for each metal ion that is bound through C or N to the cyanide ligand. As shown by the presence of low-spin hexacyano-iron species in the Mössbauer and IR spectra, a small degree (5–6%) of linkage isomerization of the bridging cyanide ligand occurs upon formation of compound **3**.

Compounds **1**, **2**, and **3** exhibit spontaneous magnetic ordering at 15.0, 13.1, and 10.1 K, respectively, but suffer from crystallographic disorder, as shown by the poor powder X-ray diffraction quality. The disorder results in the observation of spin-glass behavior, a phenomenon that is unexpected in this class of compounds. The spin-glass behavior has a significant effect on the field-dependent magnetization below T_c and T_f. Field-dependent magnetization shows several signatures that can be attributed to spin-glass behavior, such as metamagnetic behavior and magnetizations that are difficult to saturate.

The relationship between structure, disorder, and magnetic behavior is very important in this class of materials. This study has shown an example of uncommon structural and magnetic behavior found in a Prussian blue analogue made in non-aqueous conditions.

Experimental Section

All manipulations were performed under N_2 or Ar using a Vacuum Atmospheres inert atmosphere DriLab. Dichloromethane (CH_2Cl_2) was dried and distilled under N_2 from CaH_2. Acetonitrile (MeCN) was dried and twice distilled under N_2 from CaH_2. Tetrahydrofuran (THF) was dried and distilled under N_2 from sodium/benzophenone. $[(Ph_3P)_2N]_2[Mn^{IV}(CN)_6]$[9] and $[Fe^{II}(NCMe)_6][B[C_6H_3(CF_3)_2]_4\}_2$[37] were made as previously described.

Infrared spectra were recorded on either a Perkin–Elmer Model 783 or a Bio-Rad Model FTS 40 spectrophotometer with $\pm 1\,cm^{-1}$ resolution. Samples were analyzed as Nujol and Fluorolube mulls between NaCl plates. X-ray powder diffraction spectra were taken on a Rigaku Miniflex diffractometer model 1GC2 ($Cu_{K\alpha}$). The reflection 2θ values were corrected with an internal crystalline silicon standard and refinements made with a VAX-based refinement program LATPARM.

X-ray photoelectron spectra (XPS) were obtained by the use of a Fison ESCALAB model 220i-XL spectrometer with an $Al_{K\alpha}$ radiation source operated at 10 kV and 15 mA. High-resolution scans were measured with a band-pass energy of 20 eV. The X-ray beam was focused to a 100 μm spot size, while a 6–8 eV electron flood gun was used to control charging on the samples. System pressures were $\sim 7 \times 10^{-12}$ bar. The compounds were mounted on a stainless steel holder with double-sided conducting tape in a glove box and transferred under N_2 by a special transfer arm that allowed direct O_2-free loading of the sample into the spectrometer. The carbon 1s peak of the double sided conducting tape (284.6 eV) was used as a reference for binding energy shifts in the spectra.

Thermal properties of materials were studied on a TA Instruments Model 2910 differential scanning calorimeter (DSC) and a TA Model 2050 thermal gravimetric analyzer (TGA). The DSC was equipped with an LNCA liquid N_2 cooling accessory, which enabled operation between -150 and 725 °C. The TGA was also equipped with a TA-MS Fison triple-filter quadrupole mass spectrometer to identify gaseous products with masses less than 300 amu. The TGA was operated between ambient and 1000 °C and was located in a Vacuum Atmospheres inert atmosphere DriLab in order to study oxygen and moisture sensitive samples. DSC samples were weighed and hermetically sealed in aluminum pans in an argon atmosphere. TGA samples were handled in an argon atmosphere and heated under a nitrogen purge. Sample sizes were between 0.8 and 2 mg. Heating rates were 15 °C min^{-1} for TGA and 5 °C min^{-1} for DSC experiments.

^{57}Fe Mössbauer spectra were taken with a constant-acceleration type Mössbauer spectrometer. The spectrometer was equipped with a 1024-channel analyzer operating in the timescale mode, and a 25 mCi ^{57}Co/Rh source was employed. The isomer shifts reported here are relative to α-Fe at room temperature. Spectra of the samples (~ 5 mg Fe cm^{-2}) were collected at 130 K and below 20 K by means of a combined He continuous flow/bath cryostat. The Mössbauer spectra were analyzed by means of a computer program (MOSFUN[43]) using Lorentzian line shapes.

Elemental analyses were performed on freshly prepared samples hermetically sealed under argon in tin capsules and combusted in a Perkin–Elmer, model 2400 elemental analyzer. Vanadium pentoxide (LECO) was added to samples as a combustion aid in some analyses.

Magnetic susceptibility measurements were made between 2 and 300 K with a Quantum Design MPMS-5 5T SQUID magnetometer with a sensitivity of 10^{-8} emu (or 10^{-12} emu Oe^{-1} at 1 T) and was equipped with the ultra-low field (~ 0.005 Oe) accessory, reciprocating sample measurement system, and continuous low-temperature control with enhanced thermometry features. Zero-field-cooled measurements were made in a residual field of about -0.002 ± 0.001 to 0.002 ± 0.001 Oe based on the

0947-6539/99/0510-3026 $ 17.50+.50/0 *Chem. Eur. J.* **1999**, *5*, No. 10

fluxgate response. Measurements were made on powders contained in airtight Delrin® holders. The data were corrected for the measured diamagnetism of each holder used. Core diamagnetism of $Fe[Mn(CN)_6]$ was calculated from standard diamagnetic susceptibility tables giving a value of -78.4×10^{-6} emu mol^{-1}. Two equivalents of water were assumed to be incorporated into the hydrated and isomerized samples (water is apparent in the IR spectra) and included with the formula mass and diamagnetic corrections.

Synthesis of "Fe[Mn(CN)$_6$]" (1): A solution $[Fe(NCMe)_6]\{B[C_6H_3(CF_3)_2]_4\}_2$ (0.8350 g, 0.4115 mmol) in THF/CH_2Cl_2 (10 mL, 1:1) was added to a solution of $[(Ph_3P)_2N]_2[Mn(CN)_6]$ (0.5300 g, 0.4115 mmol) in CH_2Cl_2 (10 mL) in darkness. A dark green gel-like precipitate formed immediately, which was recovered by filtration and washed several times with THF and CH_2Cl_2. The filtrate was colorless. The solid was dried in vacuo at room temperature for about 12 h. A deep green solid was isolated in quantitative yield. IR (Nujol): $\tilde{\nu}_{CN}=2127$ (s), 2070 cm^{-1} (w,sh); Thermal analyses: T_{onset} 45 °C, endotherm, T_{onset} 118 °C, exotherm (DSC), T_{onset} 66 °C (TGA). Attempts at obtaining satisfactory elemental analyses by standard combustion methods were unsuccessful, as analyses of several samples ranging between about 0.5 and 1.2 mg from the same batch were inconsistent and the measured nitrogen content was approximately 12% lower than expected. V_2O_5 was added to one sample as a combustion aid, but improvement was not observed.

Synthesis of compound 2: Compound **1** was hydrated by exposure to moist air for ~1 min for IR studies, and wet MeOH for Mössbauer studies.

Synthesis of compound 3: Compound **2** was heated to 40 °C for 4 h.

Acknowledgment

We gratefully acknowledge stimulating discussions with Prof. A. J. Epstein, C. Wynn, and M. Girtu (Ohio State University), and the support from the U.S. Department of Energy (Grant No. DE FG 03-93ER45504) and in part by the American Chemical Society (Grant No. ACS-PRF #30722-AC5). J.E. and P.G. wish to thank the Fonds der Chemischen Industrie and the University of Mainz (Materialwissenschaftliches Zentrum) for financial support.

[1] a) A. L. Buchachenko, *Russ. Chem. Rev.* **1990**, *59*, 307; A. L. Buchachenko, *Usp. Khim.* **1990**, *59*, 529; O. Kahn, *Molecular Magnetism*, VCH, **1993**; b) A. Caneschi, D. Gatteschi, R. Sessoli, P. Rey, *Acc. Chem. Res.* **1989**, *22*, 392; D. Gatteschi, *Adv. Mat.* **1994**, *6*, 635; c) J. S. Miller, A. J. Epstein, W. M. Reiff, *Acc. Chem. Res.* **1988**, *21*, 114; J. S. Miller, A. J. Epstein, W. M. Reiff, *Science*, **1988**, *240*, 40; J. S. Miller, A. J. Epstein, W. M. Reiff, *Chem. Rev.* **1988**, *88*, 201; J. S. Miller, A. J. Epstein, *New Aspects of Organic Chemistry* (Eds.: Z. Yoshida, T. Shiba, Y. Ohsiro), VCH, New York, NY **1989**, p. 237; d) J. S. Miller, A. J. Epstein, *Angew. Chem.* **1994**, *106*, 399; *Angew. Chem. Int. Ed. Engl.* **1994**, *33*, 385; e) J. S. Miller, A. J. Epstein, *Adv. Chem. Ser.* **1995**, *245*, 161; J. S. Miller, A. J. Epstein, *Chem. Eng. News*, **1995**, *73*, 30.

[2] a) "Conjugated Polymers and Related Materials: The Interconnection of Chemical and Electronic Structure": J. M. Manriquez, G. T. Yee, R. S. McLean, A. J. Epstein, J. S. Miller, *Science* **1991**, *252*, 1415; b) J. S. Miller, G. T. Yee, J. M. Manriquez, A. J. Epstein, in *Proceedings of Nobel Symposium #NS-81*, Oxford University Press, **1993**, p. 461; c) "Conjugated Polymers and Related Materials: The Interconnection of Chemical and Electronic Structure": A. J. Epstein, J. S. Miller, in *Proceedings of Nobel Symposium #NS-81*, Oxford University Press, **1993**, p. 475; d) J. Zhang, P. Zhou, W. B. Brinckerhoff, A. J. Epstein, C. Vazquez, R. S. McLean, J. S. Miller, *ACS Sym. Ser.* **1996**, *644*, 311.

[3] a) W. R. Entley, G. Girolami, *Science* **1995**, *268*, 397; b) T. Mallah, S. Thiébaut, M. Verdaguer, P. Veillet, *Science*, **1993**, *262*, 1554.

[4] S. Ferlay, T. Mallah, R. Ouahes, P. Veillet, M. Verdaguer, *Nature* **1995**, *378*, 701; E. Dujardin, S. Ferlay, X. Phan, C. Desplances, C. C. dit Moulin, P. Sainctavit, F. Baudelet, E. Dartyge, P. Veillet, M. Verdaguer, *J. Am. Chem. Soc.* **1998**, *120*, 11347.

[5] V. Gadet, T. Mallah, I. Castro, M. Verdaguer, *J. Am. Chem. Soc.* **1992**, *114*, 9213.

[6] O. Sato, T. Iyoda, A. Fujishima, K. Hashimoto, *Science* **1996**, *271*, 49.

[7] F. Herren, P. Fischer, A. Ludi, W. Hälg, *Inorg. Chem.* **1980**, *19*, 956.

[8] W. E. Buschmann, J. S. Miller, submitted.

[9] a) W. E. Buschmann, C. Vazquez, M. D. Ward, N. C. Jones, J. S. Miller, *Chem. Commun.* **1997**, 409; b) This procedure was improved by using $[Fe(C_5H_5)_2][B\{C_6H_3(CF_3)_2\}_4]$ as the oxidant in MeCN to give up to 90% yield. The $[Mn^n(CN)_6]^{m-}$ $[n(m)=II(4), III(3), IV(2)]$ complexes hydrolyze immediately upon dissolution in water.

[10] a) J. R. Fowler, J. Kleinberg, *Inorg. Chem.* **1970**, *9*, 1005; b) G. Trageser, H. H. Eysel, *Z. Anorg. Allg. Chem.* **1976**, *420*, 273; c) R. Klenze, B. Kanellalopulos, G. Trageser, H. H. Eysel, *J. Chem. Phys.* **1980**, *72*, 5819.

[11] W. E. Buschmann, L. Liable-Sands, A. L. Rheingold, J. S. Miller, *Inorg. Chim. Acta* **1999**, *284*, 175.

[12] a) A. G. Sharpe, *The Chemistry of Cyano Complexes of the Transition Metals*, Academic Press, New York, **1976**, chapter 6; b) A. G. Sharpe, *The Chemistry of Cyano Complexes of the Transition Metals*, Academic Press, New York, **1976**, chapter 7.

[13] W. E. Buschmann, J. S. Miller, unpublished results.

[14] W. R. Entley, G. Girolami, *Inorg. Chem.* **1994**, *33*, 5165; W. R. Entley, G. Girolami, *Inorg. Chem.* **1995**, *34*, 2262.

[15] J. R. Armstrong, B. M. Chadwick, D. W. Jones, J. E. Sarneski, H. J. Wilde, J. Yerkess, *Inorg. Nucl. Chem. Lett.* **1973**, *9*, 1025.

[16] R. Klenze, B. Kanellakopulos, G. Trageser, H. H. Eysel, *J. Chem. Phys.* **1980**, *72*, 5819.

[17] W. E. Buschmann, A. M. Arif, J. S. Miller, *Angew. Chem.* **1998**, *100*, 813; *Angew. Chem. Int. Ed.* **1998**, *37*, 781.

[18] a) R. E. Wilde, S. N. Ghosh, B. J. Marshall, *Inorg. Chem.* **1970**, *9*, 2512; b) S. N. Ghosh, *J. Inorg. Nucl. Chem.* **1974**, *36*, 2465.

[19] E. Reguera, J. F. Bertrán, L. Nuñez, *Polyhedron* **1994**, *10*, 1619.

[20] D. B. Brown, D. F. Shriver, *Inorg. Chem.* **1969**, *8*, 37.

[21] a) D. F. Shriver, S. A. Shriver, S. E. Anderson, *Inorg. Chem.* **1965**, *4*, 725; b) D. B. Brown, D. F. Shriver, L. H. Schwartz, *Inorg. Chem.* **1968**, *7*, 77.

[22] Partial isomerization to $[Fe(CN)_x(NC)_{6-x}]$ cannot be ruled out. The Mössbauer data does not resolve an increase in an intermediate isomerization species for $[Fe(CN)_x(NC)_{6-x}]$.

[23] a) T. Mallah, S. Ferlay, C. Auberger, C. He'lary, F. L'Hermite, R. Ouah'es, J. Vaissermann, M. Verdaguer, P. Veillet, *Mol. Cryst. Liq. Cryst.* **1995**, *273*, 141; b) W. R. Entley, C. R. Treadway, G. S. Girolami, *Mol. Cryst. Liq. Cryst.* **1995**, *273*, 153; c) O. Kahn, *Molecular Magnetism*, VCH, New York, **1993**.

[24] "Magnetic Molecular Materials": V. Gadet, M. Bujoli-Doeuff, L. Force, M. Verdaguer, K. E. Malkhi, A. Deroy, J. P. Besse, C. Chappert, P. Veillet, J. P. Renard, P. Beauvillain, *NATO ASI Ser. Ser. E* **1991**, *198*, 281.

[25] a) G. W. Beall, W. O. Milligan, J. Korp, I. Bernal, *Inorg. Chem.* **1977**, *16*, 2715; b) H. J. Buser, D. Schwarzenbach, W. Petter, A. Ludi, *Inorg. Chem.* **1977**, *16*, 2704; c) H. B. Weiser, W. O. Milligan, J. B. Bates, *J. Phys. Chem.* **1942**, *46*, 99; d) J. F. Keggin, F. D. Miles, *Nature* **1936**, 577.

[26] This condition complies with the second law of thermodynamics.

[27] A. R. West, *Solid State Chemistry and its Applications*, Wiley, New York, **1984**, pp. 173–175.

[28] "Molecular Assemblies to the Devices: NATO Advanced Studies Workshop": F. Palacio, *NATO ASI Ser. Ser. E* **1996**, *321*, 5.

[29] a) *Handbook of X-Ray Photoelectron Spectroscopy* (Ed.: G. E. Muilenberg), Perkin–Elmer, Eden Prarie, Minnesota, **1978**; b) J. F. Moulder, W. F. Stickle, P. E. Sobol, K. D. Bomben, *Handbook of X-Ray Photoelectron Spectroscopy* (Eds.: J. Chastain, R. C. King, Jr.), Physical Electronics, Minnesota, **1995**.

[30] P. Gütlich, R. Link, A. Trautwein, in *Inorganic Concepts 3: Mössbauer Spectroscopy and Transition Metal Chemistry*, Springer, New York, **1988**, pp. 19, 56–77.

[31] a) K. Maer, Jr., M. L. Beasley, R. L. Collins, W. O. Milligan, *J. Am. Chem. Soc.* **1968**, *90*, 3201; b) E. König, K. Madeja, *Inorg. Chem.* **1967**, *6*, 48.

[32] The presence of $[Mn^{II}(CN)_6]^{4-}$ is unlikely because it is not seen in the XPS spectra [Mn^{II} $2p_{3/2}$ 638.3 eV[29b]] and there is no reductant, for example, Fe^{IV}, present.

[33] A. Ito, M. Suenaga, K. Ono, *J. Chem. Phys.* **1968**, *48*, 3597.

[34] a) L. H. Jones, B. I. Swanson, G. J. Kubas, *J. Chem. Phys.* **1974**, *61*, 4650; b) L. H. Jones, B. I. Swanson, *Acc. Chem. Res.* **1976**, *9*, 128; c) L. H. Jones, *Inorg. Chem.* **1963**, *2*, 777.

[35] a) H. Inoue, E. Fluck, *Z. Naturforsch.* **1983**, *38b*, 687; b) E. Fluck, H. Inoue, S. Yanagisawa, *Z. Anorg. Allg. Chem.* **1977**, *430*, 241; c) A. Calabrese, R. G. Hayes, *J. Am. Chem. Soc.* **1974**, *96*, 5054.
[36] The water content in **2** is assumed to be 2 molar equivalents (one molecule of water per cavity of the face-centered cubic lattice) for diamagnetic corrections.
[37] W. E. Buschmann, J. S. Miller, *Eur. J. Chem.* **1998**, *4*, 1731.
[38] B. N. Figgis, in *Comprehensive Coordination Chemistry Vol. 1* (Ed.: G. Wilkinson), Pergamon, New York, **1987**, pp. 256 – 274.
[39] D. C. Mattis, *The Theory of Magnetism I*, Springer, New York, **1981**; C. Kittel, *Introduction to Solid State Physics*, 5th ed., Wiley, New York, **1976**.
[40] E. J. Brandon, D. K. Rittenberg, A. M. Arif, J. S. Miller, *Inorg. Chem.* **1998**, *37*, 3376; P. Zhou, B. G. Morin, A. J. Epstein, R. S. McLean, J. S. Miller, *J. Appl. Phys.* **1993**, *73*, 6569; W. B. Brinckerhoff, B. G. Morin, E. J. Brandon, J. S. Miller, A. J. Epstein, *J. Appl. Phys.* **1996**, 79, 6147; E. J. Brandon, D. K. Rittenberg, A. M. Arif, J. S. Miller, *Inorg. Chem.* **1998**, *37*, 337.
[41] a) J. A. Mydosh, *Spin Glasses*, Taylor and Francis, Washington, DC, **1993**, chapter 1; b) J. A. Mydosh, *Spin Glasses*, Taylor and Francis, Washington, DC, **1993**, chapter 3; c) J. A. Mydosh, *Spin Glasses*, Taylor and Francis, Washington, DC, **1993**, pp. 88 – 97.
[42] A. P. Ramirez, *Ann. Rev. Mater. Sci.* **1994**, *24*, 453.
[43] MOSFUN, W. E. Müller, *Mössbauer Effect Data Journal* **1981**, *4*, 89.

Received: November 30, 1998
Revised version: March 5, 1999 [F1470]

  0947-6539/99/0510-3028 $ 17.50+.50/0